

Sivashinsky equation for corrugated flames in the large-wrinkle limit

Guy Joulin^{1,*} and Bruno Denet^{2,†}¹Laboratoire de Combustion et de Détonique, UPR 9028 du CNRS, ENSMA,
1 rue Clément Ader, B.P. 40109, 86961 Futuroscope Cedex, Poitiers, France²Institut de Recherche sur les Phénomènes Hors d'Equilibre, UMR 6594 du CNRS,

Technopole de Château Gombert, 49 rue Joliot-Curie, 13384 Marseille Cedex 13, France

(Received 31 October 2007; revised manuscript received 7 April 2008; published 23 July 2008)

Sivashinsky's [Acta Astron. 4, 1177 (1977)] nonlinear integrodifferential equation for the shape of corrugated one-dimensional flames is ultimately reducible to a $2N$ -body problem, involving the $2N$ complex poles of the flame slope. Thual, Frisch, and Hénon [J. Phys. (France) 46, 1485 (1985)] derived singular linear integral equations for the pole density in the limit of large steady wrinkles ($N \gg 1$), which they solved exactly for monocoalesced periodic fronts of highest amplitude of wrinkling and approximately otherwise. Here we solve those analytically for isolated crests, next for monocoalesced, then bicoalesced periodic flame patterns, whatever the (large) amplitudes involved. We compare the analytically predicted pole densities and flame shapes to numerical results deduced from the pole-decomposition approach. Good agreement is obtained, even for moderately large N s. The results are extended to give hints as to the dynamics of supplementary poles. Open problems are evoked.

DOI: 10.1103/PhysRevE.78.016315

PACS number(s): 47.20.Ky, 47.54.-r, 47.70.Fw, 82.40.Ck

I. INTRODUCTION

Being able to describe the nonlinear development of the Landau-Darrieus [1,2] (LD) instability of premixed-flame fronts is a central topic in combustion theory. As early as 1977 Sivashinsky [3] showed, in the limit $\mathcal{A} \ll 1$ of small Attwood numbers based upon the fresh gas (ρ_u) or burnt gas ($\rho_b < \rho_u$) densities, $0 < \mathcal{A} \equiv (\rho_u - \rho_b) / (\rho_u + \rho_b) < 1$, that the shape $\phi(x, t)$ of a flat-on-average spontaneously evolving wrinkled flame is governed by

$$\phi_t + \frac{1}{2} \phi_x^2 = \nu \phi_{xx} + I(\phi) \quad (1)$$

in suitable units. In Eq. (1) the subscripts denote partial derivatives with respect to time, t , and coordinate, x , normal to the mean direction of propagation, and the “viscosity” $\nu > 0$ represents a reciprocal Peclet number based upon the actual flame thickness and the wrinkle wavelength. The linear integral operator $I(\cdot)$ is defined by $I(e^{ikx}) = |k| e^{ikx}$ [whereby $I(\phi)$ is the Hilbert transform, $\hat{H}(-\phi_x)$, of $-\phi_x$] and stems from the LD instability. The growth and/or decay rate of infinitesimal harmonics is $|k| - \nu k^2$, which identifies $1/\nu$ and ν as neutral wave number and minimum growth time, respectively. The nonlinearity is geometrical, accounting as it does for the cosine, $(1+s^2)^{-1/2} \approx 1 - s^2/2 + \dots$, of the small angle [$\arctan(s) \approx s + \dots$] that the local normal to the flame front makes to the mean direction of propagation, where $s \sim \phi_x \times \mathcal{A}$ is the unscaled front slope. Originally derived in [3] as a leading order result for $\mathcal{A} \rightarrow 0^+$, Eq. (1) happens to govern the shape of steadily propagating fronts even when two more terms of the \mathcal{A} expansion are retained [4,5]; its structure then remains valid practically up to $\mathcal{A} = 3/4$, i.e., $\rho_u = 7\rho_b$ [4].

Numerics [6] reveals that “steady” solutions of Eq. (1), corresponding to $\phi(x, t) = -Vt + \phi(x)$ are often ultimately reached. When Eq. (1) is integrated with periodic boundary conditions for “not-too-small” values of ν , $\nu > 1/25$ say, the “steady” pattern has a single crest per x -wise interval of 2π length, where ϕ_{xx} is large and negative; without loss of generality one may assume that one is located at $x=0$, in which case $\phi_x=0$ when x is an integer multiple of π [i.e., $x=0 \pmod{\pi}$] and $\phi_{xx}(\pm\pi) \approx 1/\pi$. If Neumann conditions at $x=0$ and $x=\pi$ are used instead, still with a moderately small ν , the final pattern obtained from numerical (pseudospectral) integrations of Eq. (1) may also have an extra crest located at $x=\pi$ [7], with $\phi_{xx}(\pi)$ large and negative. By the very way they are obtained as the final state of an unsteady process the two-crested patterns have a finite basin of attraction, contrary to the case of periodic boundary conditions [7] where the only stable patterns have a single crest per cell; yet such “half-channel” solutions happen to coincide with the restriction to $0 \leq x \leq \pi$ of properly shifted 2π periodic ones, for these are symmetric about $x=0$ and $x=\pi$. If ν is too small the widest patterns become very sensitive to noise, even when caused by numerical rounding off. In [8] the estimate $\mu \geq O(e^{-1/2\nu\kappa}) \equiv \mu_c(\kappa)$ was obtained for the noise intensity μ needed to trigger the appearance of extra cells on top of the main ones with periodic boundary conditions; the number κ in the above exponent is $\phi_{xx}(\pm\pi) \approx 1/\pi$; since the most rapidly growing noise-induced disturbances (with initial wave numbers $|k| \approx 1/\nu$ [8]) of a nearly parabolic trough undergo an $O(e^{1/2\nu\kappa})$ amplification, they ultimately become visible as subwrinkles of $O(1)$ final amplitude if $\mu \geq \mu_c(\kappa)$. Having a larger $\phi_{xx} > 0$ at their troughs (see Sec. VII), two-crested patterns are presumably less sensitive to noise than the single-crest ones associated with the same wavelength because $\mu_c(\kappa)$ increases dramatically with κ when ν is small. The numerical work of Ref. [9] also showed that sums $\phi(x_1, x_2, t) = \phi_1(x_1, t) + \phi_2(x_2, t)$ of orthogonal, two-crested one-dimensional (1D) patterns play a central role in the study of Eq. (1) generalized to two-dimensional flames

*Corresponding author; joulin@lcd.ensma.fr

†bruno.denet@irphe.univ-mrs.fr

$[x \rightarrow (x_1, x_2), \phi_x^2 \rightarrow |\nabla \phi|^2, \phi_{xx} \rightarrow \Delta \phi, I(\cdot) \equiv$ multiplication by $(\mathbf{k} \cdot \mathbf{k})^{1/2}$ in the 2D Fourier space $\mathbf{k}=(k_1, k_2)]$ and to rectangular domains in the Cartesian (x_1, x_2) plane. Without noise such sums are exact stable solutions; with random additive forcing they recurrently appear as long-lived transients when Neumann conditions are adopted.

Further analyses on the stability of solutions of Eq. (1) and their responses thus seem warranted, and getting the “steady” patterns that correspond to wide, hence large, cells (or small ν s) is a prerequisite. The present contribution is intended to do this.

It is organized as follows. Section II introduces the pole-decomposition method, the discrete equations for the pole locations, and the two integral equations that approximate them for large front wrinkles. The latter equations are next solved analytically for isolated crests (Sec. III) then one-crested periodic patterns (Sec. IV), and the prediction compared to numerical results from the pole-decomposition approach. Sections V and VI compute the flame speed from the density, and take up the dynamics of a few extra poles, respectively. Section VII generalizes the above integral equations to a pair of coupled ones corresponding to two-crest periodic flames (and “half-channel” ones), then solves them analytically; comparisons with numerics are again presented. We end up with concluding remarks and open problems (Sec. VIII).

II. POLE DECOMPOSITION(S)

In 1985 Thual, Frisch, and Hénon [10] (herein referred to as “TFH”) discovered (see also [11]) that Eq. (1) possesses solutions $\phi(x, t)$ representing 2π -periodic flame patterns with slopes ϕ_x in the form

$$\phi_x(x, t) = -\nu \sum_{\alpha=-N}^N \cot\left(\frac{x - z_\alpha}{2}\right), \tag{2}$$

in which the complex-valued poles of $\phi_x(x, t)$, $z_\alpha(t)$, are involved in conjugate pairs ($z_{-\alpha} = z_\alpha^*$, $\alpha \neq 0$) for $\phi_x(x, t)$ to be real when x is. For this pole-decomposed expression to solve Eq. (1), the z'_α s ($\alpha = -N, \dots, -1, 1, \dots, N$) must evolve according to the $2N$ -body problem

$$\frac{dz_\alpha}{dt} = \nu \sum_{\substack{\beta=-N \\ \beta \neq \alpha}}^N \cot\left(\frac{z_\beta - z_\alpha}{2}\right) - i \operatorname{sgn}[\operatorname{Im}(z_\alpha)], \tag{3}$$

where $\operatorname{Im}(\cdot)$ denotes the imaginary parts of (\cdot) and the signum function [with $\operatorname{sgn}(0)=0$] accounts for the LD instability. Once Eq. (3) is solved for the pole locations, $\phi(x, t)$ is available from Eq. (2) and the wrinkling-induced excess propagation speed $V = -\langle \phi_t \rangle > 0$ follows from Eq. (1):

$$V = \frac{1}{2} \langle \phi_x^2 \rangle, \tag{4}$$

where $\langle \cdot \rangle$ stands for an average along the x coordinate; thus, V simply measures the wrinkling-induced fractional increase in flame arclength, since $\langle (1+s^2)^{1/2} - 1 \rangle = \langle s^2/2 \rangle + \dots \sim \mathcal{A}^2 \times V$. Beside periodic $\phi(x, t)$ s, Eq. (1) also allows [10] for isolated nonperiodic wrinkles that have an infinite wavelength, $V=0$, $\cot(z)$ replaced by $1/z$, and

$$\frac{dz_\alpha}{dt} = \nu \sum_{\substack{\beta=-N \\ \beta \neq \alpha}}^N \frac{2}{z_\beta - z_\alpha} - i \operatorname{sgn}[\operatorname{Im}(z_\alpha)]. \tag{5}$$

In the latter situation, the precise value of $\nu > 0$ does not matter since it could be scaled out, and the integer $N \geq 1$ is arbitrary. As for Eqs. (2) and (3), the maximum allowed value $N_{\text{opt}}(\nu)$ of N in steady configurations increases with $1/\nu > 1$ [10]. As shown by TFH, steady flames obtained from Eqs. (3) or (5) correspond to poles that “coalesce” (or align) along parallels to the imaginary axis, as a result of the pairwise pole interactions that are attractive along the real x axis and repulsive in the normal direction. In the case of an isolated crest located at $x=0$, the poles ultimately involved in steady solution are of the form iB_α , $-N \leq \alpha \leq N$, $\alpha \neq 0$, with real B_α s satisfying coupled discrete equations deduced from Eq. (5):

$$\nu \sum_{\substack{\beta=-N \\ \beta \neq \alpha}}^N \frac{2}{B_\alpha - B_\beta} = \operatorname{sgn}(B_\alpha). \tag{6}$$

The authors of Ref. [10] also evidenced that the larger the number N of pole pairs in such “vertical” steady alignments, the smoother the involved poles are distributed along the B coordinate, with $B_{\alpha+1} - B_\alpha$ much smaller than B_N . This suggested TFH to replace the discrete sum in Eq. (6) [or its analogue deduced from Eq. (3)] by an integral over the continuous variable B , with such a continuous measure that $P(B)dB$ is the number of poles located between B and $B + dB$; a constructive definition of $P(B)$ is specified in Eq. (20). In this continuous approximation the steady versions of Eqs. (2) and (3) are amenable to singular Fredholm integral equations, specifically,

$$\int \frac{2\nu P(B')}{B - B'} dB' = \operatorname{sgn}(B) \tag{7}$$

in the nonperiodic situations (an isolated wrinkle at $x=0$), and

$$\int \nu P(B') \coth\left(\frac{B - B'}{2}\right) dB' = \operatorname{sgn}(B) \tag{8}$$

for the monocoalesced 2π periodic cases [one single crest per cell, at $x=0 \pmod{2\pi}$]. In Eqs. (7) and (8) B denotes the pole imaginary coordinate, and the Cauchy principal parts $f \cdot dB'$ stem from the condition $\beta \neq \alpha$ on the sums featured in Eqs. (3) and (5). Consistent with their interpretation as pole densities, the $P(B)$ s showing up in Eqs. (7) and (8) both are non-negative even functions of their argument (for ϕ_x to be real when x is) and are normalized by

$$\int P(B') dB' = 2N. \tag{9}$$

In Eqs. (7)–(9) the integrals extend over the ranges (to be determined as part of the solutions) where $P(B) \neq 0$. The next sections will solve Eqs. (7)–(9) analytically, starting with the simpler Eq. (7).

III. ISOLATED CREST

Because isolated crests have $\phi_x \rightarrow 0$ at $|x| \rightarrow \infty$, we first anticipate the existence of some finite $B_{\max} > 0$ such that $P(|B| > B_{\max}) \equiv 0$ in Eq. (7). We next recall the identity

$$\int_{-\pi/2}^{\pi/2} \frac{\cos[(2M+1)\Phi'] \cos \Phi'}{\sin \Phi - \sin \Phi'} d\Phi' = \pi \sin[(2M+1)\Phi] \quad (10)$$

that can be deduced, through the change of variable $\Phi \rightarrow \Phi + \pi/2$, from a similar one appearing in the Prandtl theory of lifting lines [12,13]. Identity (10) allows one to solve such singular integral equations as Wigner's [14] (for the density, $2\nu P$ say, of eigenvalues of large real random matrices in the Gaussian orthogonal ensemble), written here as

$$\int \frac{2\nu P(B')}{B - B'} dB' = B; \quad (11)$$

its solution is the celebrated semicircle law $2\pi\nu P(B) = \max(B_{\max} \cos \Phi, 0)$ [14], provided that one sets

$$B = B_{\max} \sin \Phi, \quad -\frac{\pi}{2} \leq \Phi \leq \frac{\pi}{2}, \quad (12)$$

in Eq. (11). Interestingly, the same change of independent variable in Eq. (7) produces

$$\int_{-\pi/2}^{\pi/2} \frac{2\nu P(\Phi') \cos \Phi'}{\sin \Phi - \sin \Phi'} d\Phi' = \text{sgn}(\Phi), \quad (13)$$

since $\text{sgn}(B) = \text{sgn}(\Phi)$ for $|\Phi| < \pi$. Over the same range [and hence over the narrower support of P , $|\Phi| \leq \pi/2$], the right-hand side of Eq. (13) may be expanded as the Fourier series

$$\text{sgn}(\Phi) = \frac{4}{\pi} \sum_{M=0}^{\infty} \frac{1}{2M+1} \sin[(2M+1)\Phi], \quad (14)$$

consistent with our convention that $\text{sgn}(0) = 0$. From Eq. (10) the solution to Eq. (13) can thus be written as a Fourier series of cosines that all vanish at $\Phi = \pm \pi/2$:

$$2\nu P(\Phi) = \frac{4}{\pi^2} \sum_{M=0}^{\infty} \frac{1}{2M+1} \cos[(2M+1)\Phi] \quad (15)$$

$$= \frac{1}{\pi^2} \ln \left(\frac{1 + \cos \Phi}{1 - \cos \Phi} \right) \quad (16)$$

$$= \frac{1}{\pi^2} \ln \left(\frac{1 + \sqrt{1 - B^2/B_{\max}^2}}{1 - \sqrt{1 - B^2/B_{\max}^2}} \right), \quad (17)$$

and $P \equiv 0$ for $|B| > B_{\max}$; to obtain Eq. (17) from Eq. (16), Eq. (12) was explicitly employed.

The cumulative pole distribution $R(B) = \int_0^B P(B') dB'$ reads, after integration by parts,

$$2\nu R(B) = \frac{B_{\max}}{\pi^2} \left(\sin \Phi \ln \frac{1 + \cos \Phi}{1 - \cos \Phi} + 2\Phi \right), \quad (18)$$

whereby the renormalization condition $R(B_{\max}) = R(\Phi = \pi/2) = N$ fixes B_{\max} to be given by

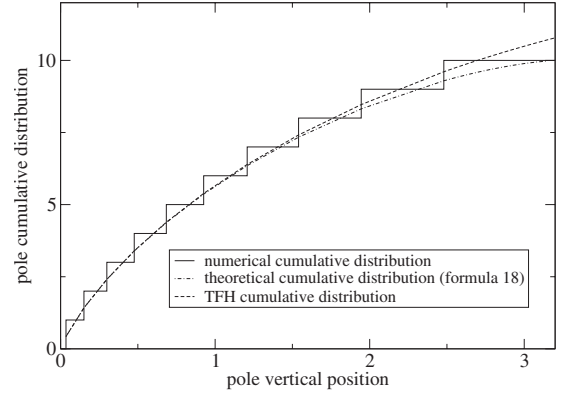


FIG. 1. Numerical vs analytical cumulative pole densities, for an isolated crest with $1/\nu = 19.5$, $N = 10$. If exact, the theoretical curve [dotted-dashed line, Eq. (18)] would pass through the middle of the risers of the numerical staircase [solid line, Eq. (5)]. The dashed line is the TFH fit.

$$B_{\max} = 2\pi N \nu. \quad (19)$$

TFH [10] fitted the cumulative distribution they obtained from a numerical resolution of Eq. (5) for steady arrangements of aligned poles, by the expression $\pi^2 \nu R = \int_0^B \ln(1.28 N \nu \pi^2 / |B'|) dB'$ when $|B| \leq B_{\max}$ [10]. Equations (17) and (19) show that 1.28 estimated from their numerical pole distribution at $|B| \ll B_{\max}$ actually was a numerical approximation of $4/\pi = 1.273\dots$. Figures 1 and 2 compare the analytical findings [Eqs. (18) and (19)] to our own resolutions of Eq. (5), with $N = 10$ and 100, respectively. The TFH fit is also displayed for illustration. The pole density P is defined for $\alpha \geq 1$ by

$$P[(B_\alpha + B_{\alpha-1})/2] \equiv (B_\alpha - B_{\alpha-1})^{-1}, \quad (20)$$

in terms of the pole locations (with $B_0 = 0$ by convention); it is shown in Fig. 3 for $N = 100$, and compared with the continuous approximation (17) and the TFH fit. Once the cumulative distribution is determined by Eqs. (18) and (19) in the continuous limit, approximations \tilde{B}_α to the discrete pole locations can be retrieved upon solving [10]

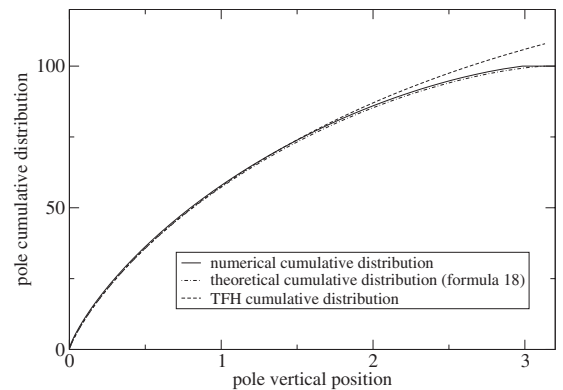


FIG. 2. Same as in Fig. 1, for $1/\nu = 199.5$, $N = 100$. Only the upper hull (solid line) of the exact staircase is shown, for readability. The dashed line is the TFH fit.

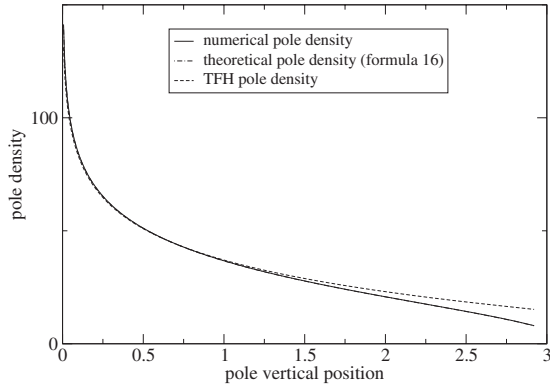


FIG. 3. Numerical [Eq. (20), solid line] vs analytical [Eq. (17), dotted-dashed line] pole densities $P(B)$ for an isolated crest with $1/\nu=199.5$, $N=100$. The dashed line is the TFH fit.

$$R(\tilde{B}_\alpha) = \alpha - 1/2, \quad \alpha = 1, \dots, N \quad (21)$$

numerically (e.g., by the Newton-Raphson method, with the “exact” B_α as an initial guess). The resulting crest shape

$$\tilde{\phi}(x) = -2\nu \sum_{\alpha=1}^N \ln \left(1 + \frac{x^2}{\tilde{B}_\alpha^2} \right) \quad (22)$$

is compared to the exact one (numerical) in Fig. 4 and to that issued from the continuous approximation. The latter profile has

$$\phi_x = - \int_{-B_{\max}}^{B_{\max}} \frac{2\nu P(B)dB}{x - iB} \quad (23)$$

$$= - \frac{1}{\pi} \operatorname{sgn}(x) \ln \left(\frac{\sqrt{x^2/B_{\max}^2 + 1} + 1}{\sqrt{x^2/B_{\max}^2 + 1} - 1} \right), \quad (24)$$

the second expression resulting from substitution of Eq. (17) in Eq. (23), then a look at p. 591 of Ref. [15].

As suggested by the form of Eq. (23), and confirmed by Eq. (24), $\phi_x(x)$ is most simply deduced from $P(\pm ix)$ through contour integration in the complex B plane. A further integration by parts of Eq. (24) yields the continuous-approximation prediction for $\phi(x)$ (up to an additive constant),

$$\phi(x) = - \frac{1}{\pi} \operatorname{sgn}(x) B_{\max} \left(\sinh \xi \ln \frac{\cosh \xi + 1}{\cosh \xi - 1} + 2\xi \right), \quad (25)$$

where $x = B_{\max} \sinh \xi$ [compare to Eq. (12)]. The integration constant was selected in Fig. 4 to achieve good agreement with the exact $\phi(x)$ for $|x| \rightarrow \infty$. Two final remarks: (i) ν disappeared as a factor in Eq. (24) as it should, because ν can be scaled out; (ii) $\phi(x)$ is of the form $\nu NF(x/\nu N)$, and this scale-invariance shows that the continuous approximation actually amounts to describing $\phi(x)$ at large distances compared to the actual radius of curvature $[1/\int_{B_1}^{B_{\max}} 4\nu P(B)dB/B^2 = o(\nu)]$ of the flame tip, when $N \gg 1$ (that is, for large wrinkles).

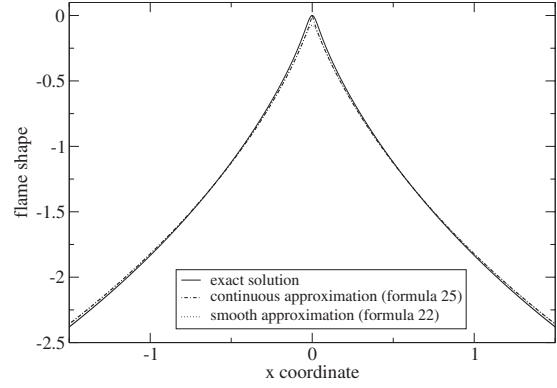


FIG. 4. Shapes of an isolated crest with $1/\nu=19.5$, $N=10$: continuous approximation [Eq. (25), dotted-dashed line], exact (solid line), and smooth approximation from Eq. (22) (dotted).

IV. MONOCOALESCED PERIODIC CREST

The following simple remark will allow us to solve Eq. (8), i.e., in the case where all the poles of ϕ_x are aligned along the imaginary x axis (mod 2π). Because $P(B')$ still is an even function of B' , only the even parts (at fixed B) of $\coth[(B-B')/2]$ will actually contribute to the integral over B' . Equation (8) may thus be rewritten as

$$\int_{-B_{\max}}^{B_{\max}} \frac{\nu P(B') [1 - \tanh^2(B'/2)]}{\tanh(B/2) - \tanh(B'/2)} dB' = \operatorname{sgn}(B), \quad (26)$$

upon use of the known formula for the $\tanh(\cdot)$ of a difference, and neglect of a term proportional to $\int P(B') \tanh(B'/2) dB' = 0$. We now set

$$\tanh\left(\frac{B}{2}\right) = \tanh\left(\frac{B_{\max}}{2}\right) \sin \Phi, \quad -\frac{\pi}{2} \leq \Phi \leq \frac{\pi}{2}, \quad (27)$$

converting Eq. (26) into

$$\int_{-\pi/2}^{\pi/2} \frac{2\nu P(B') \cos \Phi'}{\sin \Phi - \sin \Phi'} d\Phi' = \operatorname{sgn}(\Phi), \quad (28)$$

which is nothing but Eq. (13). Therefore the sought after pole density is still given by Eq. (16), the only difference with the previous nonperiodic case being that B , B_{\max} , and Φ are now related by Eq. (27) instead of Eq. (12).

The new cumulative density $R(B) = \int_0^B P(B') dB'$ is given, after an integration by parts, by

$$\begin{aligned} \pi^2 \nu R(B) &= \frac{1}{2} \ln \frac{1 + A \sin \Phi}{1 - A \sin \Phi} \ln \frac{1 + \cos \Phi}{1 - \cos \Phi} \\ &+ \int_0^\Phi \ln \frac{1 + A \sin \Phi'}{1 - A \sin \Phi'} \frac{d\Phi'}{\sin \Phi'}, \end{aligned} \quad (29)$$

$A \equiv \tanh(B_{\max}/2)$, whereby the normalization (9) requires

$$N \nu \pi^2 = \int_0^{\pi/2} \ln \frac{1 + A \sin \Phi}{1 - A \sin \Phi} \frac{d\Phi}{\sin \Phi}. \quad (30)$$

As the above integral turns out to be $\pi \arcsin A$ (p. 591 of [15]) the range of $P(B)$, still given by $R(B_{\max}) = N$, now satisfies

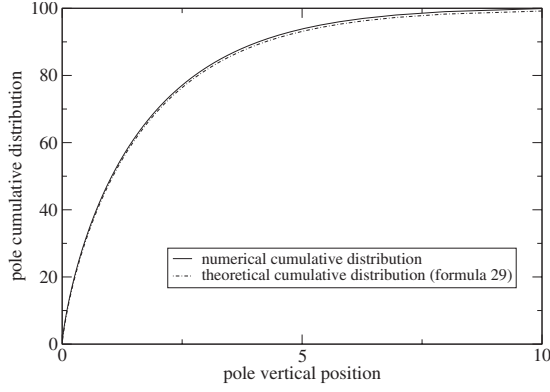


FIG. 5. Numerical (solid line) vs analytical [Eq. (29), dotted-dashed line] cumulative pole densities for a monoalesced periodic crest, for $1/\nu=199.5$ and $N=100 [=N_{\text{opt}}(\nu)]$. Only the upper hull of the numerical staircase is shown.

$$\tanh(B_{\text{max}}/2) = \sin(\pi N \nu) \quad (31)$$

instead of Eq. (19). The latter and Eq. (31) coincide for $\pi N \nu \ll 1$, as do the associated pole densities. The maximum B_{max} allowed by Eq. (31), $B_{\text{max}} = +\infty$, has $2N\nu=1$ and $\cos \Phi \equiv 1/\cosh(B/2)$, where $P(B)$ resumes the form

$$P(B) = \frac{1}{\pi^2 \nu} \ln \left(\coth \frac{|B|}{4} \right) \quad (32)$$

obtained by TFH *via* Fourier transformations. Figure 5 compares our predictions, Eqs. (29) and (31), with very accurate solutions of Eq. (3) for $N=100$ and $2N\nu=1$. Very good agreement is obtained even if N is only moderately large, and carries over to the pole densities themselves. Again, approximate solutions \tilde{B}_α can be retrieved from the analog of Eq. (21), and an approximate flame front shape from

$$\tilde{\phi}(x) = -2\nu \sum_{\alpha=1}^N \ln(1 - \cos x \operatorname{sech} \tilde{B}_\alpha) + \text{const.} \quad (33)$$

Figure 6 shows a comparison between Eq. (33), the exact flame shape obtained from the exact (yet obtained numeri-

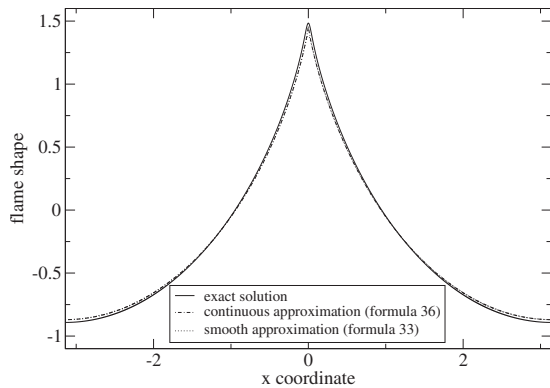


FIG. 6. Shapes of a monoalesced periodic flame with $1/\nu=19.5$, $N=10 [=N_{\text{opt}}(\nu)]$: continuous approximation [Eq. (36), dotted-dashed curve] vs exact result (solid line) and smooth approximation [Eq. (33), dotted].

cally) B_α s satisfying Eq. (3), and the curve deduced from the continuous approximation, for which the flame slope $\phi_x(x)$ reads

$$\phi_x = -\nu \int \cot \left(\frac{x-iB}{2} \right) P(B) dB, \quad (34)$$

again a real function because $P(-B)=P(B)$. With $P(B)$ given by Eqs. (16), (27), and (31) the above integral can be reduced to one available in p. 591 of [15] and yields (for $-\pi \leq x \leq \pi$)

$$\phi_x(x) = -\frac{1}{\pi} \operatorname{sgn}(\xi) \ln \frac{\cosh \xi + 1}{\cosh \xi - 1}, \quad \tan \frac{x}{2} \equiv A \sinh \xi, \quad (35)$$

thereby confirming that $\phi_x(x)$ is accessible from $P(B)$ by analytical continuation to $\pm ix$. In particular, the TFH solution, Eq. (32), has $\pi \phi_x = -2 \operatorname{sgn}(x) \ln |\cot x/4|$ and $\phi_{xx}(\pm \pi) = 1/\pi$; more generally, $\phi_{xx}(\pm \pi) = A/\pi$. A further integration by parts yields

$$\begin{aligned} -i\pi \phi(x) &= \operatorname{sgn}(x) \ln \frac{1+iA \sinh \xi}{1-iA \sinh \xi} \ln \frac{\cosh \xi + 1}{\cosh \xi - 1} \\ &+ 2 \operatorname{sgn}(x) \int_0^\xi \ln \frac{1+iA \sinh \xi'}{1-iA \sinh \xi'} \frac{d\xi'}{\sinh \xi'}, \end{aligned} \quad (36)$$

which cannot be evaluated in simple closed form, but may be compared to Eq. (29); of course $\phi(x)$ is real when x is, since the complex $\ln(\cdot)$ in Eq. (36) also reads $2i \arctan(A \sinh \xi) = ix$. Note that $\phi(x)$ has the form $F(x; N\nu)$, in the present units where the pattern is 2π periodic. Adopting $\Lambda \neq 2\pi$ as a wavelength would give $2\pi \phi = \Lambda F(2\pi x/\Lambda; 2\pi N\nu/\Lambda)$ with the same F . Accordingly, if $\nu N/\Lambda$ is kept fixed, $\phi_{xx}(\pm \Lambda/2)$ scales similar to $1/\Lambda$, as it should for $\nu \rightarrow 0$, whereby halving the wavelength renders the patterns less sensitive to noise (see the Introduction).

V. FLAME SPEED FROM CONTINUOUS POLE DENSITY

Plugging Eq. (34) into Eq. (4) allows the wrinkling-induced increase in flame speed V to be written as

$$2V = \nu^2 \iint P(B) P(B') \left\langle \cot \frac{x-iB}{2} \cot \frac{x-iB'}{2} \right\rangle dB dB'. \quad (37)$$

Although the one-variable integrals involved when squaring Eq. (34) are ordinary ones, they may be written as principal parts. We next invoke the trigonometric identity $\cot a \cot b = -1 + \cot(a-b)(\cot b - \cot a)$ and the average

$$\left\langle \cot \frac{x-iB}{2} \right\rangle = i \operatorname{sgn}(B) \quad (38)$$

to transform Eq. (37) into

$$2\frac{V}{\nu^2} = - \int \int P(B)P(B')dBdB' + 2 \int \int \operatorname{sgn}(B)P(B)P(B')\coth\left(\frac{B-B'}{2}\right)dB'dB \tag{39}$$

The first double integral $\{=\int P(B)dB\}^2$ in Eq. (39) follows from the normalization (9), and is $(2N)^2$. The second one is obtained from Eq. (8) after multiplication of both sides by $P(B)\operatorname{sgn}(B)dB$ and subsequent integration over B : by Eq. (9), it is $2N/\nu$. Thus the simple formula

$$V = 2N\nu(1 - N\nu) \tag{40}$$

ensues; notice that it was obtained without having to solve Eq. (8). Actually Eq. (39) can be shown from Eq. (3) to hold whatever N and ν [16], again without solving the pole equations themselves.

In view of the accuracy of Eq. (40) one may inquire whether the solutions of Eqs. (7) and (8) satisfy the ‘‘inviscid’’ Sivashinsky equation, i.e., Eq. (1) with $\nu=0$, in the steady cases. To show they do, for $x \neq 0$ at least, one may set $\mathcal{P} = P\nu$ and $\mathcal{N} = N\nu$ to remove ν from Eqs. (7) and (9), then process the Landau-Darrieus term of Eq. (1) as follows in the case of an isolated crest:

$$\begin{aligned} 2iI(\phi) &= \int \frac{4\mathcal{P}(B)\operatorname{sgn}(B)}{x-iB}dB \\ &= \int \frac{2\mathcal{P}(B)}{x-iB}dB \int \frac{2\mathcal{P}(B')}{B-B'}dB' + (B \leftrightarrow B') \\ &= \int \int \frac{4i\mathcal{P}(B)\mathcal{P}(B')}{(x-iB)(x-iB')}dBdB' \\ &= i\phi_x^2, \end{aligned} \tag{41}$$

where the notation $(B' \leftrightarrow B)$ represents a second copy of the integral that precedes it, with B and B' interchanged. The lines above successively use Eq. (7), acknowledge that (B, B') are dummy variables of integration that may be interchanged, then employ Eq. (23) squared. Hence Eq. (25) satisfies Eq. (1) when $\nu=0$ and \mathcal{N} is prescribed, if $x \neq 0$. Thanks to Eq. (39), a similar analysis applies to Eq. (8), provided $x \neq 0 \pmod{2\pi}$.

Besides providing one with an exact $P(B)$, Eq. (16) shows that Eq. (8) admits a continuum of solutions, for there exists nothing in Eq. (9) to tell one that N ought to be an integer; this will be commented on later (see Sec. VIII). One finally specializes Eq. (8) to $B=B_{\max}$ to show that N is constrained by $0 \leq 2N\nu \leq 1$, since $\coth(B_{\max}-B) \geq 1$ [see also Eq. (31)].

VI. DYNAMICS OF SUPPLEMENTARY POLE PAIRS

In 2000, Vaynblatt and Matalon [17] addressed the linear stability of pole-decomposed monocoalesced ‘‘steady’’ solutions $-Vt + \phi(x)$ to Eq. (1). Upon writing $\phi(x, t) + Vt - \phi(x) \sim \exp(\omega t)\psi_\omega(x) \ll 1$ then analytically solving the linearized dynamics to obtain ω and $\psi_\omega(x)$, the authors of [17] identified two types of linear modes. The modes of type I describe

how the $2N$ poles of $\phi_x(x)$ evolve when displaced by infinitesimal amounts from equilibrium; all those are stable ($\omega < 0$), but one that has $\omega = 0$ (see below). The modes of type II were interpreted [17,18] as resulting from x -periodic arrays of poles at $\pm i\infty$ that may spontaneously approach the real axis if N is too small for the selected $\nu < 1$. The overall conclusion was thus: when endowed with 2π -periodic boundary conditions, all the monocoalesced solutions are linearly unstable, except a single one that has $N = N_{\text{opt}}(\nu) \equiv \lfloor (1 + 1/\nu)/2 \rfloor \approx 1/2\nu$ ($\lfloor \cdot \rfloor \equiv$ integer part) and is neutrally stable ($\omega = 0$) against shifts along the x axis, the corresponding anti-symmetric eigenmode being $\psi_0(x) = \phi_x(x)$. For $N < N_{\text{opt}}$, modes of type II can manifest themselves, two particularly dangerous ones corresponding to incipient secondary wrinkles centered on the main crests ($x = 0, \text{ mod } 2\pi$) or troughs ($x = \pi, \text{ mod } 2\pi$).

When Neumann conditions are employed instead, the aforementioned shifts are not allowed any longer because $\psi_{0x} \neq 0$ at $x = 0$ and $x = \pi$. Numerical integrations [7] of Eqs. (1) and (3) evidence that there may then exist stable bicoalesced patterns comprising an extra crest located at $x = \pi$. Even though the steady 2π -periodic patterns also satisfy Eq. (1) with Neumann conditions when properly shifted to have $\phi_x(0) = 0 = \phi_x(\pi)$, no stability analysis similar to [17] is yet available in this case; yet instabilities then necessarily require $N < N_{\text{opt}}(\nu)$. Here we address a restricted aspect of the problem, namely: we study how the previously determined monocoalesced ‘‘steady’’ solutions (25) and (36) interact with extra pairs of poles. Since the free dynamics (3) conserves the total number of pole pairs at its $t=0$ value, it makes sense to consider $\phi(x, 0)$ that involve them in a larger number ($N+n$) than the $N = O(1/\nu)$ ones retained in a steady profile $\phi(x)$. Each of the n supplementary pairs at $x_m(t) \pm iy_m(t)$ contributes a perturbation $\phi_m(x, t) = \langle \phi_m \rangle - 4\nu \sum_{j \geq 1} \times \exp(-j|y_m|)\cos[j(x-x_m)]/j$ to the flame shapes [this follows from Eq. (2) via a term-by-term Fourier expansion [10]] and, as shown in [18], superposing ϕ_m s can reproduce virtually any disturbance $\phi(x, 0) - \phi(x)$. In the present formulation the only difference between Neumann and 2π -periodic boundary conditions deals with the initial phases $x_m(0)$: whereas the former require the x_m s to be compatible with the $x \leftrightarrow -x$ and $\pi - x \leftrightarrow \pi + x$ symmetries, the latter do not.

Contrary to the more conventional normal-mode method (to which it is equivalent if $|y_m(0)| \gg 1$ [18]), the pole approach can follow the disturbances when significant nonlinear effects set in...if one is able to solve the $2N+2n$ coupled equations for the pole trajectories in the complex plane. The next remark somewhat simplifies the task. In the limits $N \gg 1$, $\nu \rightarrow 0^+$ and $\nu N = O(1)$ that led to Eq. (8), accounting for $n = O(1)$ extra pole pairs—as is assumed here—exerts only a small $O(\nu)$ perturbation on the $2N$ poles already aligned. Accordingly the distribution $P(B)$ of poles along the main alignments at $x = 0 \pmod{2\pi}$ may be kept unchanged, and given by Eqs. (16), (27), and (31), when computing the motion of $2n$ supplementary ones.

In the illustrative examples that follow only two extra poles ($n=1$) located at $\pm iy(t) \pmod{2\pi}$, $y > 0$, then at $\pi \pm iy(t)$ are considered, to begin with.

A. Extra poles at $x \approx 0 \pmod{2\pi}$

When the two supplementary poles are located at $\pm iy(t) \pmod{2\pi}$, their altitude $y(t)$ is determined from Eq. (3)—within $O(\nu, 1/N)$ fractional errors in the limits $N \gg 1$, $\nu \rightarrow 0^+$ and $\nu N = O(1)$ —by the ordinary differential equation (ODE)

$$\frac{dy}{dt} = \int \nu P(B') \coth\left(\frac{y-B'}{2}\right) dB' - 1 \quad (42)$$

$$= \frac{2}{\pi} \arcsin[\sin(\pi N \nu) \coth(y/2)] - 1, \quad |y| \geq B_{\max}, \quad (43)$$

where $P(B)$ is the *same* as given by Eqs. (16), (27), and (31), to leading order, and leads to the closed form (43) on integration [15]; for $|y| \leq B_{\max}$, $dy/dt = 0$ by Eq. (8). Therefore, whenever $0 < 1 - 2\nu N = O(1)$ and $\nu \rightarrow 0^+$, any initial $y(0) > B_{\max}$ will ultimately lead to $y(+\infty) = B_{\max}^+$, thereby adding one new incomer to the already present continuum. Put in words: if $2\nu N < 1$ initially, the main pattern is unstable to disturbances with poles at $\pm iy(t)$, and the latter process tends to make $2N\nu$ approach 1 from below.

Periodic boundary conditions would allow the supplementary pair to be initially off the x axis, say at $x(0) \pm iy(0)$ with $0 < x(0) < \pi \pmod{2\pi}$. The “horizontal” attraction by the main pole condensation at $x=0$ [$O(\nu)$, actually] [10] will make $x(t)$ decrease, while $y(t)$ still does if $2N\nu < 1$. Ultimately, the extra pole pair will join the main pole alignment (in finite time), and the previous conclusion is qualitatively unchanged: the process makes N increase by one. When Neumann conditions are adopted, however, at least *two* pairs $\pm x(t) \pm iy(t)$ are needed if $x(t) \neq 0$, to meet the requirement of symmetry about $x=0$, and two possibilities are encountered as to their fate. In the first instance, corresponding to not-too-small $x(0)$ s and moderate values of $y(0)$, the process is qualitatively the same as above, except that two pairs simultaneously join the main condensation at $|y| < B_{\max}$, thereby making N increase by 2. If $x(0)$ is small and $y(0)$ well above B_{\max} , the horizontal mutual attraction between the pair members may make them hit the $x=0$ axis at such a finite time t_c that $y(t_c) > B_{\max}$; this is best shown from Eq. (3) specialized to $x(t) \ll 1$, whereby $dx/dt \approx -\nu/x$ then $x^2(t) + 2\nu(t-t_c) \approx 0$ for $t \leq t_c$. The double pole thus formed at $iy(t_c)$ then instantly splits into two simple ones lying on the $x=0$ axis at $y(t) - y(t_c) \sim \pm (t-t_c)^{1/2}$, leading to a subsequent dynamics that ultimately ends similar to the beginning of this section if $2N\nu < 1$.

B. Extra poles at $x \approx \pi \pmod{2\pi}$

In case the supplementary poles are located at $\pi \pm iy(t)$, Eq. (42) is replaced by

$$\frac{dy}{dt} = \frac{2}{\pi} \arcsin[\sin(\pi N \nu) \tanh(y/2)] - 1 + \nu \coth y, \quad (44)$$

since $\coth(u + i\pi/2) = \tanh u$. Even though $\nu \ll 1$ the last term in Eq. (44), stemming from the interaction of the extra pole with its complex conjugate, cannot be simply discarded, for otherwise Eq. (44) would not be uniformly valid if y be-

comes small. According to Eq. (44), any initial $y(0)$ indeed ultimately leads to $y(+\infty) = \nu + o(\nu)$ and to a small [$O(\nu)$] stable disturbance centered at $x = \pi \pmod{2\pi}$ whenever $2N\nu < 1$. Although the main pattern's curvature $\phi_{xx}(\pi) > 0$ is $O(1)$, and the $O(\nu)$ contribution to $\phi(x, t)$ of the extra pole pair is small, it is nevertheless enough [7] to render the flame shape $\phi(x, t)$ concave downward at $x = \pi$; as shown in [7], this occurs as soon as the extra poles enter a thin strip about the real axis, $|y| \lesssim \sqrt{4\pi\nu}$. Incorporating $O(N)$ extra pairs will also do, but the process of dynamical trough splitting is not within reach of such ODEs as Eqs. (44) when $n = O(N)$. The structure of two-crested steady patterns with $n = O(N)$ will be studied in Sec. VII.

Like in Sec. VI A one might begin generalizing the present discussion by envisaging a single pair of extra poles off the $x = \pi$ axis, but this is already covered in the preceding paragraphs: if $0 < x(0) < \pi$ the pair ultimately joins the poles at $x=0 \pmod{2\pi}$. It is more revealing to consider two such pairs at $\pi \pm x(t) \pm iy(t)$ with $x(t)$ “small enough,” in a way compatible with Neumann conditions, because something new appears. Comparatively large $x(0)$ s will clearly lead to pairs that ultimately stick at $x=0 \pmod{2\pi}$ because their mutual horizontal attraction could not oppose that of the main alignments. The other extreme of very small $x(0)$ again leads to the formation of double poles at some $\pi \pm iy(t_c)$, then a subsequent evolution of the two pairs $\pi \pm iy_{1,2}$ along the line $x = \pi \pmod{2\pi}$ until they settle at $O(\nu)$ distances to the real axis if $2N\nu < 1$. The important conclusion is that stable two-crest patterns exist when Neumann conditions are used and $2N\nu < 1$.

By continuity there exist separating trajectories S_{\pm} , such that none of the above behaviors is observed if the pole pairs initially sit on them. The lines S_{\pm} lead the two supplementary pairs towards an unstable equilibrium, a result of a competition between attraction by the main pole population at $x=0 \pmod{2\pi}$, and the mutual attractions and/or repulsions among the pair members. For $\nu \ll 1$, and $N\nu = O(1)$, using the steady version of Eq. (3) and the pole density given by Eqs. (16), (27), and (31), one can show that such equilibria correspond to $x(+\infty) = \pm (2\pi\nu/A)^{1/2} + \dots$ and $y(+\infty) = \pm \nu + \dots$ to leading order, again with $A = \tanh(B_{\max}/2) = \sin(\pi N \nu)$. This shows that there exist even more general steady solutions than considered elsewhere in the paper and in the literature (except in [7] where a similar conjecture was made on a numerical basis). One could have included other pairs as well, some of which along the $x = \pi \pmod{2\pi}$ axis.

Our last remark is to again stress that the free dynamics (3) conserves the total number of poles (if finite). By the same token, allowing this number to vary with time is a means to study a *forced* version of the Sivashinsky equation: adding a pair of poles $x_m \pm iy_m$ at $t = t_m$ amounts to accounting for a term $\phi_m(x) \delta(t - t_m)$ in the right-hand side of Eq. (1), and combining many ϕ_m s with various phases (as to vary their signs), amplitudes [$\approx -4\nu \exp(-|y_m|)$ if $|y_m| \gg 1$] and times of implantation (t_m) could help one investigate the response of flames to a rich class of weak random noises. We understand that a similar proposal was developed about the “kicked” Burgers equation [19], i.e., Eq. (1) without the integral term in the one-dimensional case.

VII. BICOALESCED PERIODIC PATTERNS

We now take up the structure of “steady” 2π -periodic solutions of Eq. (1) that would have N pairs of poles iB_α (mod 2π), $\alpha = \pm 1, \pm 2, \dots, \pm N$, and $n = O(N)$ other pairs at $\pi + ib_\gamma$ (mod 2π), $\gamma = \pm 1, \pm 2, \dots, \pm n$. For brevity, we will say that the pole alignments reside “at” $x=0$ or $x=\pi$, respectively, such as the two crests per cell they correspond to. Because $\coth(u+i\pi/2) \equiv \tanh(u)$, the steady versions of Eq. (3) corresponding to such bicoalesced flame patterns read as

$$\nu \sum_{\substack{\beta=-N \\ \beta \neq \alpha}}^N \coth\left(\frac{B_\alpha - B_\beta}{2}\right) + \nu \sum_{\delta=-n}^n \tanh\left(\frac{B_\alpha - b_\delta}{2}\right) = \text{sgn}(B_\alpha), \tag{45}$$

$$\nu \sum_{\substack{\delta=-n \\ \delta \neq \gamma}}^n \coth\left(\frac{b_\gamma - b_\delta}{2}\right) + \nu \sum_{\beta=-N}^N \tanh\left(\frac{b_\gamma - B_\beta}{2}\right) = \text{sgn}(b_\gamma). \tag{46}$$

In the distinguished limits $\nu \rightarrow 0^+$, $N\nu = O(1)$, $n\nu = O(1)$, the poles at $x=0$ and $x=\pi$ are densely packed (at the scale of the wavelength), with densities $P(B)$ and $p(b)$, respectively. Both P and p will be non-negative and, in general, compactly supported: $P(|B| \geq B_{\max}) = 0 = p(|b| \geq b_{\max})$. The ranges B_{\max} and b_{\max} are to be found as part of the solutions to the continuous versions of Eqs. (45) and (46),

$$\int \nu P(B') \coth\left(\frac{B - B'}{2}\right) dB' + \int \nu p(b') \tanh\left(\frac{B - b'}{2}\right) db' = \text{sgn}(B), \tag{47}$$

$$\int \nu p(b') \coth\left(\frac{b - b'}{2}\right) db' + \int \nu P(B') \tanh\left(\frac{b - B'}{2}\right) dB' = \text{sgn}(b), \tag{48}$$

that are valid for $|B| \leq B_{\max}$ and $|b| \leq b_{\max}$, respectively. To restore some symmetry we set

$$\tanh(B/2) = A \sin \Phi, \quad A \equiv \tanh(B_{\max}/2) \leq 1, \tag{49}$$

$$\tanh(b/2) = a \sin \varphi, \quad a \equiv \tanh(b_{\max}/2) \leq 1, \tag{50}$$

in Eqs. (47) and (48), then acknowledge that both $P(\cdot)$ and $p(\cdot)$ are even functions, which allows one to suppress some odd parts of the integrands, viewed as functions of Φ' (or φ') at fixed Φ (or φ). Some cumbersome algebra ultimately transforms Eqs. (47) and (48) into

$$\begin{aligned} & \int \frac{2\nu P(\Phi') \cos \Phi'}{\sin \Phi - \sin \Phi'} d\Phi' + Aa \sin \Phi \\ & \times \int \frac{2\nu p(\varphi') \cos \varphi'}{1 - A^2 a^2 \sin^2 \varphi' \sin^2 \Phi} d\varphi' \\ & = \text{sgn}(\Phi), \end{aligned} \tag{51}$$

$$\begin{aligned} & \int \frac{2\nu p(\varphi') \cos \varphi'}{\sin \varphi - \sin \varphi'} d\varphi' + Aa \sin \varphi \\ & \times \int \frac{2\nu P(\Phi') \cos \Phi'}{1 - A^2 a^2 \sin^2 \Phi' \sin^2 \varphi} d\Phi' \\ & = \text{sgn}(\varphi), \end{aligned} \tag{52}$$

where all the variables (Φ, Φ') , (φ, φ') are now taken in the common $[-\pi/2, \pi/2]$ range. One may thus adopt a common notation for them, (σ, σ') say, in both Eqs. (51) and (52) and subtract the results to eliminate the $\text{sgn}(\cdot)$ functions in the right-hand sides. This produces an homogeneous equation for the difference $P(\cdot) - p(\cdot)$, of which one obvious solution is $P - p \equiv 0$. Hence the important result: if $P = p$ is indeed a viable solution, then

$$P(B) = J\left[\sigma = \arcsin\left(\frac{\tanh B/2}{A}\right)\right], \tag{53}$$

$$p(b) = J\left[\sigma = \arcsin\left(\frac{\tanh b/2}{a}\right)\right], \tag{54}$$

where $J(\sigma)$ is the *same* function for both. The even $J(\cdot)$ function itself is then found from Eqs. (51) or (52) to satisfy

$$\begin{aligned} & \int_{-\pi/2}^{\pi/2} \frac{2\nu J(\sigma') \cos \sigma'}{\sin \sigma - \sin \sigma'} d\sigma' + Aa \\ & \times \int_{-\pi/2}^{\pi/2} \frac{2\nu J(\sigma') \sin \sigma \cos \sigma'}{1 - A^2 a^2 \sin^2 \sigma' \sin^2 \sigma} d\sigma' = \text{sgn}(\sigma). \end{aligned} \tag{55}$$

Further changing the independent variable to θ , with

$$\sin \theta = \frac{(1 + Aa) \sin \sigma}{1 + Aa \sin^2 \sigma}, \tag{56}$$

fortunately converts the seemingly hopeless (55) into a form equivalent to the already solved Eq. (28), θ playing the part that the former Φ did there [most easily shown by starting from Eq. (28)]. Accordingly, the solution to Eq. (55) is available in terms of the already found pole density pertaining to the isolated crests, then the monocoalesced ones: from Eq. (16) one indeed has

$$2\nu J(\sigma) = \frac{1}{\pi^2} \ln \frac{1 + \cos \theta}{1 - \cos \theta}, \tag{57}$$

with θ defined in Eq. (56). As said earlier, Eqs. (53) and (54), $P(B)$ is immediately retrieved upon setting $\sin \sigma = \tanh(B/2) \coth(B_{\max}/2)$ in Eqs. (56) and (57); the same operation is used to obtain $p(b)$ from $J(\sigma)$, upon setting $\sin \sigma = \tanh(b/2) \coth(b_{\max}/2)$ in Eqs. (57) and (56).

The first step to obtain B_{\max} and b_{\max} again is to compute the cumulative pole densities. For example $R(B) = \int_0^B P(B') dB'$ is computed as follows from Eqs. (57) and (56):

$$2\pi^2 \nu R(B) = \int_0^\Phi \ln\left(\frac{1 + \cos \theta'}{1 - \cos \theta'}\right) \frac{2A \cos \Phi' d\Phi'}{1 - A^2 \sin^2 \Phi'}, \tag{58}$$

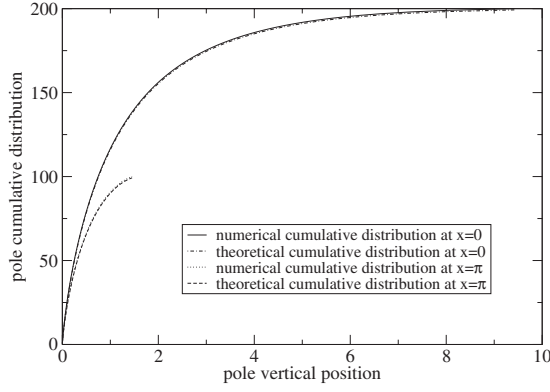


FIG. 7. Cumulative pole densities $R(B)$ (upper curves) and $r(b)$ for a bicoalesced periodic pattern with $1/\nu=600.5$, $N=200$, $n=100$: the solid and the dotted lines are from Eqs. (53), (54), (57), and (56); the dashed and the dotted-dashed ones are the upper hulls of the exact staircases (see Fig. 1). As $(N+n)=N_{\text{opt}}(\nu)$, $B_{200}=\infty$.

$$= \ln \frac{1+A \sin \Phi}{1-A \sin \Phi} \ln \frac{1+\cos \theta}{1-\cos \theta} + 2 \int_0^{\theta(\Phi)} \frac{d\theta'}{\sin \theta'} \ln \frac{1+A \sin \Phi'}{1-A \sin \Phi'}, \quad (59)$$

again with the understanding that Φ (or Φ') is viewed as a function of θ (or θ') via Eq. (56), and conversely; Eq. (58) is obtained from the definition of $R(B)$ upon setting $\tanh(B/2)=A \sin \Phi$, and Eq. (59) results from an integration by parts. The cumulative density pertaining to $p(b)$ is obtained in the same way from Eqs. (57) and (56), now thanks to $\tanh(b/2)=a \sin \varphi$: the result is similar to Eq. (59), except for the substitutions $A \rightarrow a$, $\Phi \rightarrow \varphi$, $B \rightarrow b$, $R(B) \rightarrow r(b)$. The normalizations $R(B_{\text{max}})=N$ and $r(b_{\text{max}})=n$ thus impose the two conditions

$$N\nu\pi^2 = \int_0^{\pi/2} \frac{d\theta}{\sin \theta} \ln \frac{1+A \sin \Phi}{1-A \sin \Phi}, \quad (60)$$

$$n\nu\pi^2 = \int_0^{\pi/2} \frac{d\theta}{\sin \theta} \ln \frac{1+a \sin \varphi}{1-a \sin \varphi}, \quad (61)$$

that may be compared to the former equation (30), and reduce to it when $Aa=0$. Although we could not compute the above normalization integrals in closed forms, this can be done numerically without difficulty to obtain A and a as function of $N\nu$ and $n\nu$ (or conversely). Note that $N \geq n$ is equivalent to $A \geq a$. $N > n$ also implies that $R(\cdot) > r(\cdot)$ when both are evaluated at the same argument, Fig. 7.

Before closing this section, it remains to compare the above predictions to direct numerical resolutions of Eqs. (45) and (46) by the Newton-Raphson method. This is done in Figs. 7 and 8. Figure 8 will hopefully convince the reader that both $P(B)$ and $p(b)$ can be expressed in terms of the single function $J(\sigma)$ given by Eq. (57).

Now that the pole densities are available, one may try to compute the corresponding increase in flame speed, V , from

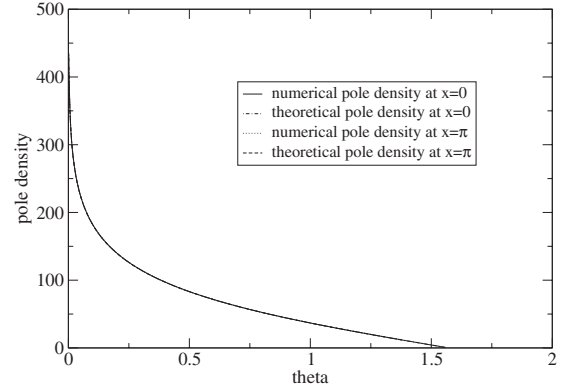


FIG. 8. Theoretical pole densities $P(B)$ [respectively, $p(b)$] plotted as dotted-dashed or dashed lines vs θ , Eq. (57), with $\sin \sigma$ replaced by $(\tanh B/2)/A$ [respectively $(\tanh b/2)/a$]. The solid and the dotted lines are the numerical pole densities. All are for a bicoalesced periodic flame with $N=200$, $n=100$, $1/\nu=600.5$.

Eqs. (47) and (48) without solving them (such as in Sec. V), to produce

$$V = 2\nu(N+n)[1 - (N+n)\nu]; \quad (62)$$

this simple formula reduce to Eq. (40) if $n=0$, and could have been deduced directly from the discrete pole equations, without solving them. The sum $N+n$ plays the part N did for monocoalesced patterns and, as is shown upon specializing Eq. (47) to $B=B_{\text{max}}$, has to satisfy $2(N+n)\nu \leq 1$.

As mentioned earlier, the flame slope $\phi_x(x)$ pertaining to the continuous approximation(s) can be obtained directly from the corresponding pole density(ies) via an analytical continuation from the real B (or b) axis to $\pm ix$. Using the same procedure here gives, for $0 \leq x \leq \pi$,

$$\phi_x = -\frac{1}{\pi} \text{sgn}(\bar{x}-x) \ln \frac{\cosh \psi + 1}{\cosh \psi - 1}, \quad (63)$$

$$\sinh \psi = \frac{(1+Aa)\tan x/2}{A-a \tan^2 x/2} \quad (64)$$

for bicoalesced flames, \bar{x} being the point where $\sinh^2 \psi \rightarrow \infty$ in Eq. (64) and, therefore, $\phi_x(\bar{x})=0$,

$$\bar{x} = 2 \arctan \sqrt{\frac{\tanh B_{\text{max}}/2}{\tanh b_{\text{max}}/2}}. \quad (65)$$

At the flame front trough, $\kappa = \phi_{xx}(\bar{x}) = 2(A+a)/\pi(1+Aa) > A/\pi$: the corresponding critical noise amplitude $\mu_c(\kappa)$ needed to trigger the appearance of subwrinkles markedly exceeds that pertaining to monocoalesced fronts (see Sec. I). Two extra pole pairs initially placed at the points $\pm \bar{x} \pm i\nu \pmod{2\pi}$ would stay there in unstable equilibrium. There exist separating trajectories S_{\pm} passing through them, which delineates the basins of attraction of the main pole condensations at $x=0$ or $x=\pi$. Only the trajectories of initially remote extra poles that are close enough to S_{\pm} will enter the $O(\sqrt{\nu})$ strip adjacent to the $B=0$ axis where their direct influence on the main pattern becomes visible [7]. As seen from the real axis, the process then manifests itself as extra

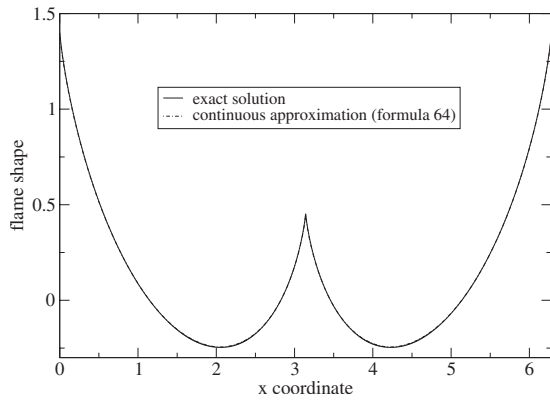


FIG. 9. Shapes of a bicoalesced flame with $1/\nu=199.5$, $N=80$, $n=20$: exact (solid line) vs continuous approximation [from integration of Eq. (63), dotted-dashed line].

sharp subwrinkles seemingly “emitted” suddenly at $x \approx \pm \bar{x} \pmod{2\pi}$ before traveling to one of the main cusps where they eventually join a main condensation. The N/n -dependent shape of such separating trajectories thus controls the fate of “supplementary” poles of whatever origin, initial conditions or forcing; this will be exploited elsewhere, though one can already confirm that stable two-crest steady patterns with $n=O(N) \sim 1/\nu$ exist if Neumann conditions are employed. With 2π -periodic conditions these are unstable even if $2\nu(N+n)=1$, as is seen by considering initial conditions where the $2n$ poles are slightly shifted to the left of $x=\pi \pmod{2\pi}$: both crests will ultimately merge.

Comparisons with accurate numerical resolutions of the pole equations (45) and (46) are again good, see Fig. 9. For $\nu=1/199.5$, $N=80$, $n=20$ they yield $\bar{x}=2.053\,973$, whereas our prediction (65), with A and a iteratively obtained from the normalization conditions (60) and (61), gives $\bar{x}=2.053\,888$. Similar to $R(B)$ and $r(b)$, $\phi(x)$ cannot be obtained in closed form, yet is readily accessible numerically. Also, if $A=a$, elementary trigonometry shows that the predicted flame slope (63) resumes the result (35), up to a two-fold reduction in x and B_{\max} scales.

VIII. CONCLUDING REMARKS AND OPEN PROBLEMS

The above analyses may convey the feeling that the pole densities obtained so far have a family likeness, which is true because they were all deduced from the solution (16) pertaining to isolated crests via adequate changes of independent variable. Whereas Eq. (16) itself basically follows from standard Fourier analysis combined with a lucky resummation of the series thus obtained (15), it would be interesting to understand why the changes of variable (27) then (56) work so well. Admittedly the integral equation (26) bears some formal resemblance with Eq. (7), which guided us to propose the variable (27); but that introduced in Eq. (56) looks more strange to us, and was actually discovered by trial and error after the “resolvent” integral equation (55) is obtained. Yet Eq. (56) unlikely solely comes “out of the blue.” In effect, one may note that Eq. (56) is equivalent to $\tanh(\beta) = \tanh(\beta_{\max}) \sin \theta$ if one defines $\tanh^2(\beta_{\max}) \equiv \tanh(B_{\max}/2)$

$\times \tanh(b_{\max}/2)$ and sets $\tanh(\beta/2) = \tanh(\beta_{\max}/2) \sin \sigma$, which clearly mirrors what was employed to map the mono-coalesced periodic case onto the isolated-crest problem. Hence Eq. (56) rests on the celebrated composition law for hyperbolic tangents (τ_1, τ_2) : $\tau_1 * \tau_2 = (\tau_1 + \tau_2)/(1 + \tau_1 \tau_2)$. It would be interesting to know whether the associated group properties give access to still more general solutions to the Sivashinsky equation (1). That the scale-invariant signum function featured in Eqs. (7) and (8) is left unchanged by the successive changes of variables also is a key property that traces back to the presence of the Hilbert transform $\hat{H}(-\phi_x)$ in Eq. (1): *in fine*, it expresses that the complex velocity about the flame is a sectionally analytic function in the complex x plane, which is indeed a robust statement for it is little affected by conformal changes of variables that would leave the real axis globally invariant.

Normalizing $P(B)$ to $2N$ brings about the grouping $N\nu$ and, as long as the integral equations (7) and (8) of the continuous approximation are concerned, there is no reason why N should be an integer. Thus, Eqs. (7) and (8) effectively admit a one-parameter continuum of solutions. The situation is, in a sense, analogous to the Saffman-Taylor problem of viscous fingering and related ones (see [20] and the references therein): when surface effects (here curvature) are omitted, a continuum of steady patterns is found. Equation (1) for flames is peculiar, however, because one knows from the very beginning that only a discrete set of steady mono-coalesced solutions exist, corresponding to N 's that are integers less than a well-defined ν -dependent value, $N_{\text{opt}}(\nu)$. The Sivashinsky equation (1) thus offers the opportunity to see how the WKB approaches to finger-width selection developed [20] for the Saffman-Taylor problem, or kin, can be transposed to the present system to obtain a quantization condition on $N\nu$; for here “inviscid” solutions are now available and one knows the answer in advance. This analysis likely is a key step to study flame response to noise, but has not yet been completed. Because WKB approaches essentially look for solutions of a linearized equation in the form $\exp[i\int^x k(x') dx']$, where $k(x) = O(1/\nu)$ depends on the “inviscid” solution, it is seen that obtaining the latter to leading $[O(1)]$ order in ν is not enough. Hence the question: how to compute the leading $[O(\nu)]$ correction to the flame profiles obtained above? Obviously this would require to better understand the nature of the continuous approximation leading to the integral equations (7)–(9) or Eqs. (47) and (48) for pole densities. In this context one may perhaps adopt the—rather unusual—view point that the exact pole equations (5), once specialized to $z_\alpha = iB_\alpha$ and steady patterns, constitute Gauss-like quadrature formulas to evaluate Eq. (7) numerically. How to define a “best” way of choosing the pivotal values, i.e., the B_α 's, naturally leads [21] to the notion of orthogonal polynomials associated with the Sivashinsky equation (1). In the case of Wigner’s equation (11) the Hermite polynomials are invoked [14], but we are not aware of such mathematical analyses about Eq. (1) and Eqs. (7) and (8).

Next, we recall that two-crested patterns studied in Sec. VII also belong to a continuous family of solution profiles, now indexed by two independent parameters $N\nu, n\nu$. Even if

$N+n$ is assumed to be given by the optimum value $N_{\text{opt}}(\nu) \approx 1/2\nu$, there still remains the question of how N/n is selected in numerical resolutions of Eq. (1) with Neumann conditions at $x=0, \pi$. The ratio N/n can undoubtedly be chosen by the initial flame shape $\phi(x,0)$. In the case of forced propagations, the noise intensity (μ) might well also play a role, for one can imagine situations where $\exp(-\pi/2\nu) \ll \mu \ll \exp(-\pi/4\nu)$: the noise is then intense enough to break mono-coalesced patterns (see Introduction), yet too weak to noticeably affect the more curved two-crested patterns with $N=n$.

To tailor a global criterion as to compare the two-crest patterns and their response to noise, the following remarks could be of some use. Let us collectively denote the B_α s and b_γ s as \mathbf{B} and \mathbf{b} , respectively. The unsteady versions of Eqs. (45) and (46)—the pole equations for bicoalesced patterns—may be rewritten as

$$\frac{d\mathbf{B}}{dt'} = -\nabla_{\mathbf{B}}U, \quad \frac{d\mathbf{b}}{dt'} = -\nabla_{\mathbf{b}}U, \quad (66)$$

in terms of $U(\mathbf{B}, \mathbf{b}) = V(\mathbf{B}) + v(\mathbf{b}) + w(\mathbf{B}, \mathbf{b})$, with

$$V(\mathbf{B}) = \nu \sum_{\alpha} |B_{\alpha}| - 2\nu^2 \sum_{\alpha, \beta < \alpha} \ln \left| \sinh \frac{B_{\alpha} - B_{\beta}}{2} \right|, \quad (67)$$

$$w(\mathbf{B}, \mathbf{b}) = -2\nu^2 \sum_{\gamma, \beta} \ln \left(\cosh \frac{b_{\gamma} - B_{\beta}}{2} \right), \quad (68)$$

and an expression similar to Eq. (67) for $v(\mathbf{b})$; $t' = t/\nu$ is time scaled by the shortest growth time of small-scale wrinkles (see Introduction). Accordingly, when the right-hand sides of Eq. (66) are supplemented with statistically identical inde-

pendent random (e.g., Gaussian) additive forcings, the joint probability density of (\mathbf{B}, \mathbf{b}) will tend to a quantity $\sim \exp[-U(\mathbf{B}, \mathbf{b})/\mu^2]$, where $\mu \ll 1$ characterizes the noise intensities. Because $U \sim 1$ in the small- ν limit [since $P(B)$ and $p(b)$ are $O(1/\nu)$] the above exponential is strongly peaked about the steady solutions. One can thus think of employing the N/n -dependent scalar $U(\mathbf{B}, \mathbf{b})$, evaluated at steady state, as an objective means to discriminate the various two-crested patterns in the presence of forcing. The task of evaluating U in the continuous approximation has not yet been completed. Neither is the analysis required to handle situations where the poles are slightly misaligned yet still symmetric about $x=0$ and $x=\pi$ for compatibility with Neumann boundary conditions.

One must finally stress that the present analyses did not exhaust all the possibilities of “steady” solutions of Eq. (1), even with 2π as minimal periodicity. The *interpolating solutions* discovered in [7,22] constitute another class, comprising (possibly many) extra poles, nearly evenly distributed [17,18] along sinuous curves at a distance from the real axis. In our opinion such unstable equilibria are also worth analyzing in detail for $\nu \rightarrow 0$, as are those mentioned in Sec. VI and generalizations of Eq. (1) itself [23].

As an end to a numerical work on Eq. (1), with noise included in the right-hand side [7], one of us concluded that “...it is likely that new analytical studies of the Sivashinsky equation should be possible: even if the equation is now almost 30 years old, many things remain to be explained.” The words still hold true.

ACKNOWLEDGMENT

One of us (G.J.) thanks H. El-Rabii (Poitiers University) for discussions and help.

-
- [1] L. D. Landau, *Acta Physicochim. URSS* **19**, 77 (1944).
 [2] G. Darrieus, work presented at La Technique Moderne, Paris, 1938 (unpublished).
 [3] G. I. Sivashinsky, *Acta Astron.* **4**, 1177 (1977).
 [4] K. A. Kazakov, *Phys. Fluids* **17**, 032107 (2005).
 [5] G. I. Sivashinsky and P. Clavin, *J. Phys. (France)* **48**, 193 (1987).
 [6] D. N. Michelson and G. I. Sivashinsky, *Acta Astron.* **4**, 1207 (1977).
 [7] B. Denet, *Phys. Rev. E* **74**, 036303 (2006).
 [8] G. Joulin, *J. Phys. (France)* **50**, 1069 (1989).
 [9] B. Denet, *Phys. Rev. E* **75**, 046310 (2007).
 [10] O. Thual, U. Frisch, and M. Hénon, *J. Phys. (France)* **46**, 1485 (1985).
 [11] Y. Lee and H. Chen, *Phys. Scr.* **2**, 41 (1982).
 [12] L. Landau and E. Lifschitz, *Fluid Mechanics* (Pergamon Press, Oxford, 1979).
 [13] G. K. Batchelor, *An Introduction to Fluid Dynamics* (Cambridge University Press, Cambridge, 1967).
 [14] M. L. Mehta, *Random Matrices*, 2nd ed. (Academic Press, Boston, 1991).
 [15] I. S. Gradshteyn and I. M. Ryzhik, *Table of Integrals, Series and Products*, 7th ed. (Elsevier-Academic Press, Amsterdam, 2007).
 [16] G. Joulin, *Combust. Sci. Technol.* **53**, 315 (1987).
 [17] D. Vaynblatt and M. Matalon, *SIAM J. Appl. Math.* **60**, 703 (2000).
 [18] O. Kupervasser, Z. Olami, and I. Procaccia, *Phys. Rev. E* **59**, 2587 (1999).
 [19] J. Bec, U. Frisch, and K. Khanin, *J. Fluid Mech.* **416**, 239 (2000).
 [20] P. Pelcé, *Théorie des Formes de Croissance* (CNRS Editions—EDP Sciences, Paris, 2000).
 [21] G. E. Andrews, R. Askey, and R. Roy, *Special Functions* (Cambridge University Press, Cambridge, 2000).
 [22] L. F. Guidi and D. H. U. Marchetti, *Phys. Lett. A* **308**, 162 (2003).
 [23] G. Joulin, *Zh. Eksp. Teor. Fiz.* **100**, 428 (1991).